WP-25-001

ASSESSMENT OF ESTIMATION METHODS FOR THE WET-BULB GLOBE TEMPERATURE

ABERDEEN TEST CENTER
DUGWAY PROVING GROUND
ELECTRONIC PROVING GROUND
REAGAN TEST SITE
REDSTONE TEST CENTER
WHITE SANDS MISSILE RANGE
YUMA PROVING GROUND

NAVAL AIR WARFARE CENTER AIRCRAFT DIVISION PATUXENT RIVER
NAVAL AIR WARFARE CENTER WEAPONS DIVISION CHINA LAKE
NAVAL AIR WARFARE CENTER WEAPONS DIVISION POINT MUGU
NAVAL SURFACE WARFARE CENTER DAHLGREN DIVISION
NAVAL UNDERSEA WARFARE CENTER DIVISION KEYPORT
NAVAL UNDERSEA WARFARE CENTER DIVISION NEWPORT
PACIFIC MISSILE RANGE FACILITY

96TH TEST WING
412TH TEST WING
ARNOLD ENGINEERING DEVELOPMENT COMPLEX

SPACE LAUNCH DELTA 30
SPACE LAUNCH DELTA 45

NATIONAL AERONAUTICS AND SPACE ADMINISTRATION

DISTRIBUTION A: APPROVED FOR PUBLIC RELEASE
DISTRIBUTION IS UNLIMITED

This page intentionally left blank.

WP-25-001

ASSESSMENT OF ESTIMATION METHODS FOR THE WET-BULB GLOBE TEMPERATURE

April 2025

Prepared by

METEOROLOGY GROUP

Published by

Secretariat
Range Commanders Council
U.S. Army White Sands Missile Range
New Mexico 88002-5110

This page intentionally left blank.

Table of Contents

Table of Figures

Table of Tables

Preface

The Range Commanders Council Meteorology Group conducted a campaign in 2021 to collect data associated with the wet-bulb globe temperature (WBGT), the standard metric for heat stress in the DoD. A predecessor paper (RCC Document WP-23-001) covered WBGT measurement platform development, data collection procedures, and data quality analysis. This paper shows the results from an assessment of the most widely used methods of estimating the black globe temperature and natural wet-bulb temperature and the resultant WBGT. The paper also offers improved estimation algorithms utilizing standard meteorological variables that are developed from the 2021 dataset. These new estimations can be applied at any location with requisite temperature, humidity, wind speed, and solar radiation data. Please direct any questions to:

Secretariat, Range Commanders Council
ATTN: TEWS-EDR
Building 1510
White Sands Missile Range, New Mexico 88002-5110
Telephone (575) 678-1107, DSN 258-1107
E-mail rcc-feedback@trmc.osd.mil

This page intentionally left blank.

Acronyms

AFB	Air Force Base
ATC	Aberdeen Test Center
BG	black globe
CL	China Lake
CRTC	Cold Regions Test Center
CS	Campbell Scientific
DPG	Dugway Proving Ground
EDW	Edwards Air Force Base
EGL	Eglin Air Force Base
HEN	Hennepin West Mesonet
HM	Hunter and Minyard
LST	local standard time
MAE	mean absolute error
MG	Meteorology Group
NCECO	North Carolina ECONet
NDFD	National Digital Forecast Database
NWB	natural wet-bulb
NWS	National Weather Service
PMRF	Pacific Missile Range Facility
RH	relative humidity
RCC	Range Commanders Council
RTC	Redstone Test Center
SFB	Space Force Base
VBG	Vandenberg Space Force Base
WBGT	wet-bulb globe temperature
WSTC	White Sands Test Center
YPG	Yuma Proving Ground

This page intentionally left blank.

1. Introduction

The effects of heat on individual and unit readiness in the DoD can lead to reductions in operational tempo and potential mission failure. In the 2019-2023 period, over 12,000 heat-related illnesses occurred within active component Service members.[1] Hazardous heat conditions can also be experienced by many civilian personnel, especially those in occupations with high percentage of outdoor exposure.[2] Developed in the mid-1950s to help reduce heat-related casualties at Marine Corps training bases[3], the wet-bulb globe temperature (WBGT) is the DoD standard for assessing heat stress conditions and formulating work-rest guidelines.[4,5,6] This index accounts for the effects of temperature, humidity, wind, and solar radiation intensity on the human body. The WBGT is determined using Equation 1.

$$WBGT = 0.1T_a + 0.2T_g + 0.7T_{nwb} \qquad \text{Equation 1}$$

where T_a is the air temperature
T_g is the black globe (BG) temperature (the temperature in the middle of a six-inch copper sphere painted matte black)
T_{nwb} is the natural wet-bulb (NWB) temperature (the temperature on a thermometer fitted with a wetted wick and aspirated naturally)

Specialized equipment is required to measure the WBGT with most installations only having one location taking readings that represent conditions across the entire installation. Bioenvironmental or biomedical staff are typically responsible for the measurements, though several DoD test ranges have meteorological staff completing the task. Enlisted personnel may also take WBGT measurements to assess heat conditions on a local scale for training and operational units. Given the size and varying environments of many installations and challenges in using the specialized equipment, interest has grown in estimating the WBGT using standard meteorological data from weather observation stations or numerical weather prediction models. Many estimation algorithms for WBGT and its components have been developed, though datasets used to verify the estimations are limited in temporal and/or geographic scope. To fill

[1] Maule, A. L., K. D. Scatliffe-Carrion, K. S. Kotas, J. D. Smith, and J. F. Ambrose. “Heat exhaustion and heat stroke among active component members of the U.S. Armed Forces, 2019-2023.” In *Medical Surveillance Monthly Report*, vol. 31, no. 4, pp. 3-8. April 2024.

[2] Bureau of Labor Statistics, U.S. Department of Labor. It’s summer and it’s hot on the job. https://www.bls.gov/opub/ted/2024/its-summer-and-its-hot-on-the-job.htm. 20 June 2024. Retrieved 22 January 2025.

[3] Yaglou, C. P. and D. Minard. *Prevention of heat casualties at Marine Corps Training Centers*. Office of Naval Research Physiology Branch report, 48 pp. 31 May 1956. Retrieved 22 January 2025. Available at https://apps.dtic.mil/sti/tr/pdf/AD0099920.pdf.

[4] Department of the Air Force. “Thermal Stress Program.” DAFI 48-151. 2 May 2022. May be superseded by update. Retrieved 22 January 2025. Available at https://static.e-publishing.af.mil/production/1/af_sg/publication/dafi48-151/dafi48-151.pdf.

[5] Department of the Army. “Heat stress control and heat casualty management.” TB MED 507. May be superseded by update. Retrieved 22 January 2025. Available at https://armypubs.army.mil/epubs/DR_pubs/DR_a/ARN35159-TB_MED_507-000-WEB-1.pdf.

[6] Department of the Navy. “Prevention of Heat and Cold Stress Injuries (Ashore, Afloat, and Ground Forces).” Chapter 3 in *Manual of Naval Preventive Medicine*. NAVMED P-5010-3. 12 February 2009. Retrieved 22 January 2025. Available at https://www.med.navy.mil/Portals/62/Documents/BUMED/Directives/All%20Pubs/5010-3.pdf.

the dearth of observations, the Range Commanders Council (RCC) Meteorology Group (MG) conducted a campaign in 2021 to collect WBGT data across different climate regions over an extended period using the same or similar sensors. (RCC WP-23-001, hereafter *Finding Improvements*)[7]

This paper covers the evaluation of the most widely used estimation algorithms for WBGT and its components and the development of algorithms that improve estimations based on the 2021 MG campaign data. Section 2 provides a description of the campaign data used for algorithm evaluation. The assessment of current and improved estimations for T_g and T_{nwb} and resultant WBGT is covered in Section 3. Section 4 discusses considerations when applying the algorithms. Section 5 provides a summary of this study.

2. Data for Algorithm Assessment

Campaign participants from 11 RCC ranges and two outside organizations over different climate regions (Figure 1) collected one- or five-minute average observations of incoming solar radiation, air temperature, relative humidity (RH), atmospheric pressure, wind speed, T_g, T_{nwb}, and WBGT within the 15 May-15 October 2021 period. The preferred height for all measurements was 4 ft above ground level (AGL), which corresponds to the average human mid-torso level and provides the best representation of conditions affecting the entire human body. Three locations collected data at 2 m AGL, the standard surface level for meteorological measurements and numerical weather prediction model output. Five locations measured WBGT at both 4 ft and 2 m AGL (Figure 2), though only one of the levels is used in the dataset for estimation evaluation.

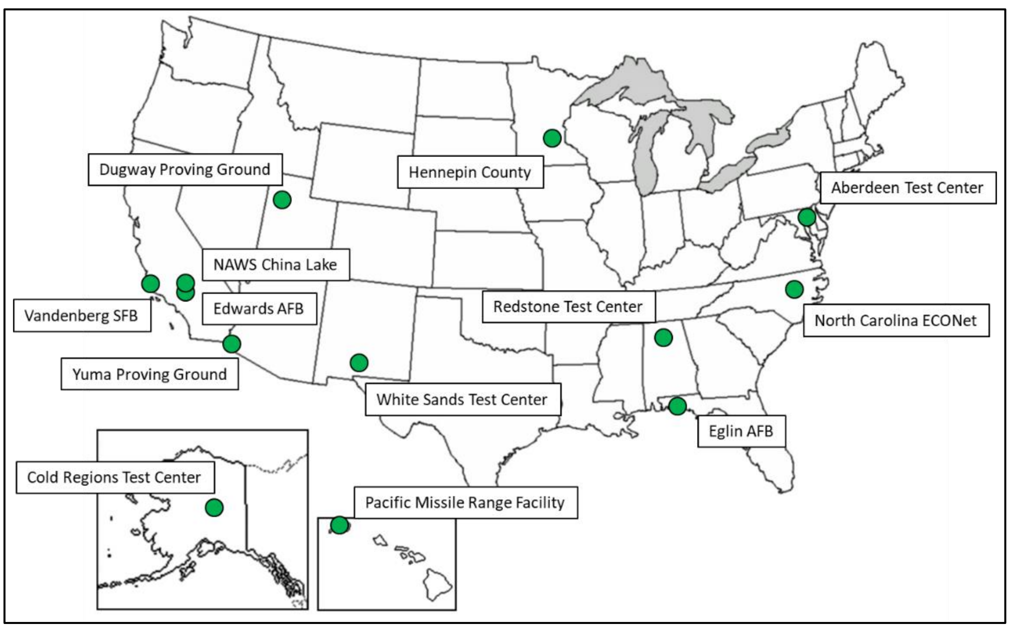

Figure 1. WBGT Data Collection Campaign Participants in 2021

[7] Range Commanders Council. *Finding improvements in the measurement and estimation of wet-bulb globe temperature*. RCC WP-23-001. August 2023. Retrieved 16 January 2025. Available at https://www.trmc.osd.mil/wiki/x/XQBSDg.

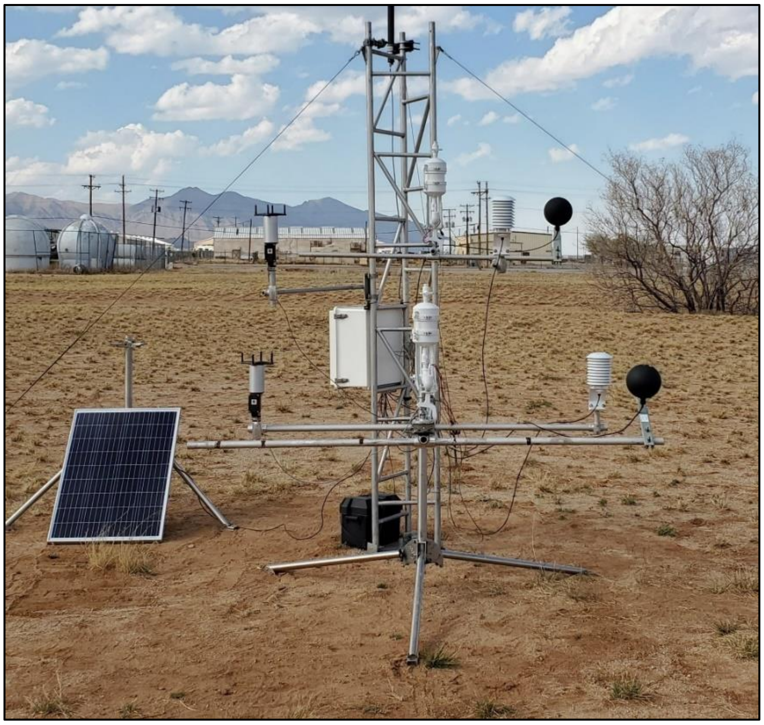

Figure 2. WBGT Measurement Platform at WSTC

The one- or five-minute average data were passed through initial quality control using procedures described in *Finding Improvements*. Fifteen-minute averages were then determined at 0, 15, 30, and 45 minutes past the hour. All one- or five-minute observations in the 15-minute period needed to be available with all measurements passing quality control for the 15-minute average to be included in the final evaluation dataset. A 15-minute average was used to temper the effects of sensor lag and smooth out data noise, both of which are more pronounced with the BG as shown in *Finding Improvements*. Additional manual inspection was done to discard suspect data not detected by the quality control checks and to adjust data showing correctable systematic biases. The number of 15-minute observations used for the assessment of T_g, T_{nwb}, and WBGT estimations is given in Table 1.

Table 1. Fifteen-Minute Observation Counts in 2021

Participant	Period of Record	Total BG Obs	Total NWB Obs	Total WBGT Obs	Notes
Aberdeen (ATC)	15 May – 01 Oct	12,354	12,353	12,353	
China Lake (CL)	15 May – 15 Oct	8649	13,186	8051	d,h
Cold Regions (CRTC)	20 May – 20 Sep	10,043	10,007	9998	i
Dugway (DPG)	11 Jun – 11 Oct	10,089	-----	-----	c
Edwards (EDW)	17 May – 15 Oct	13,535	12,210	12,210	a
Eglin (EGL)	06 Jul – 15 Oct	8445	7494	7494	
Hennepin (HEN)	10 Jun – 27 Sep	-----	9192	-----	a,b,e,g
NC ECONet (NCECO)	15 May – 15 Oct	13,730	13,096	13,096	
Pacific Missile Range Facility (PMRF)	08 Jul – 01 Aug	2175	2175	2175	
Redstone (RTC)	15 May – 15 Oct	-----	8758	-----	a,b,f
Vandenberg (VBG)	15 May – 15 Oct	14,044	14,043	14,043	
White Sands (WSTC)	15 May – 15 Oct	14,183	13,715	13,715	

Yuma (YPG)	15 May – 15 Oct	14,570	14,473	14,473	
Total		**121,871**	**130,702**	**107,608**	

[a] Measurements at 2 m AGL
[b] BG excluded due to incorrect probe positioning
[c] NWB excluded due to uncorrectable high bias
[d] NWB adjusted upward 0.8 °C for systematic bias starting 11 JUN
[e] NWB adjusted upward 0.5 °C for systematic bias throughout the period of record
[f] NWB adjusted downward 0.7 °C for systematic bias starting 11 AUG
[g] 10 m AGL wind downscaled to 2 m AGL using power-law and stability classes as in Liljegren et al. (2008)
[h] BG excluded from sunrise to 1300 local standard time (LST) due to shadowing on the sensor
[i] Name change to Arctic Regions Test Center in May 2024

3. Estimation Algorithm Assessment

Many estimation algorithms for T_g, T_{nwb}, and WBGT can be found in peer-reviewed literature, conference papers, and internal reports. For this paper, the most widely used algorithms will be evaluated: Liljegren et al.[8] (referred to as Lil) and Dimiceli and Piltz[9] (referred to as Dimiceli) for T_g; and Liljegren et al., Hunter and Minyard[10] (referred to as HM), and Bernard and Pourmoghani[11] (referred to as BP) for T_{nwb}. This paper will also evaluate additional T_g and T_{nwb} algorithms found in *Finding Improvements* along with new algorithms with improved T_g and T_{nwb} estimations introduced herein. Various combinations of T_g and T_{nwb} estimations to calculate WBGT will then be compared against measured WBGT.

The Liljegren method is the basis for the WBGT estimation calculator provided by the U.S. Occupational Safety and Health Administration (OSHA)[12] and has been used extensively in studies of WBGT magnitude and trends. Several papers[13,14,15] have noted the WBGT from Liljegren to be the most accurate when compared to other estimation methods used in those studies. The combination of T_g in the original Dimiceli paper and T_{nwb} from Hunter and Minyard were used by the U.S. National Weather Service (NWS) for WBGT estimates in its National Digital Forecast Database (NDFD) through June 2022.[16] A modified version of the Dimiceli BG

---

[8] Liljegren, J. C., R. A. Carhart, P. Lawday, S. Tschopp, and R. Sharp. "Modeling the Wet Bulb Globe Temperature Using Standard Meteorological Measurements." In *J. Occup. Environ. Hyg*., vol. 5, pp. 645-655. 4 August 2008.
[9] Dimiceli, V. E. and S. F. Piltz. "Estimation of black globe temperature for calculation of the WBGT Index." National Weather Service internal technical paper. Retrieved 22 January 2025. Available at https://www.weather.gov/media/tsa/pdf/WBGTpaper2.pdf.
[10] Hunter, C. and C. Minyard. "Estimating Wet Bulb Globe Temperature Using Standard Meteorological Measurements." WSRC-MS-99-00757. U.S. Department of Energy, Office of Scientific and Technical Information, Oak Ridge, TN. 1999. Retrieved 22 January 2025. Available at https://digital.library.unt.edu/ark:/67531/metadc620263/m1/
[11] Bernard, T. E., and M. Pourmoghani. "Prediction of workplace wet bulb global temperature." In *Appl. Occup. Environ. Hyg*., vol. 14 issue 2, pp. 126–134.
[12] OSHA. "Heat Stress." Section III, Chapter 4 in *OSHA Technical Manual*. Retrieved 22 January 2025. Available at https://www.osha.gov/otm/section-3-health-hazards/chapter-4.
[13] Lemke., B. and T. Kjellstrom. "Calculating workplace WBGT from meteorological data: A tool for climate change assessment." In *Ind. Health*, vol. 50, pp. 267-278. 2012.
[14] Patel, T., S. P. Mullen, and W. R. Santee. "Comparison of methods for estimating wet-bulb globe temperature index from standard meteorological measurements." In *Military Med.*, vol. 178, pp. 926-933. August 2013.
[15] Wodzicki, K. R. et al. "Heat stress metrics, trends, and extremes in the southeastern United States." In *J. App. Meteor. Climatol.*, vol. 63, issue 10, pp. 1137-1156. 01 October 2024.
[16] Timothy R. Boyer. "NDFD wet bulb globe temperature algorithm and software design." NWS Meteorological Development Laboratory. 8 pp. Retrieved 22 January 2025. Available at https://vlab.noaa.gov/documents/6609493/7858379/NDFD+WBGT+Description+Document.pdf.

method and the T_{nwb} estimation in *Finding Improvements* were then implemented by the NWS after demonstrated improvements in estimations were provided by the RCC-MG. The T_{nwb} estimation from BP is utilized in the most widely used handheld WBGT monitors in the U.S.[17]

3.1 BG temperature

The Liljegren BG algorithm is a physical model based on the heat energy balance of a globe (Equation 2). The balance equation can be solved for T_g by iterative methods using T_a as the first guess.

$$T_g = \left(\frac{1}{2}(1+\varepsilon_a)T_a^4 - \frac{h}{\varepsilon_g \sigma}\left(T_g - T_a\right) + \frac{S}{2\varepsilon_g \sigma}\left(1-\alpha_g\right)\left[1 + \left(\frac{1}{2\cos\theta} - 1\right) f_{db} + \alpha_{sfc}\right] \right)^{0.25} \qquad \text{Equation 2}$$

where

T_g = globe temperature (K)
ε_a = thermal emissivity of the air
T_a = air temperature (K)
h = convective heat transfer coefficient (W m^{-2} K^{-1})
ε_g = BG emissivity
σ = Stefan-Boltzmann constant
S = incoming solar radiation (W m^{-2})
α_g = BG albedo
f_{db} = direct beam radiation fraction (from 0 to 1)
θ = sun zenith angle (degrees)
α_{sfc} = surface albedo

Values for ε_a, ε_g, α_g, α_{sfc}, f_{db}, and h assigned in Liljegren et al. are used in the calculations for this paper. Wind speed is accounted for in the value of h.

The Dimiceli BG model is also derived from a heat balance equation for a globe, but the equation (taken from Hunter and Minyard) has different energy gain and heat transfer coefficient terms than those in Liljegren. Dimiceli simplified the heat balance equation to a linear expression (Equation 3), resulting in direct computation of T_g.

$$T_g = \frac{B + CT_a + 7680000}{C + 256000} \qquad \text{Equation 3}$$

where

[17] Carter, A. W., B. F. Zaitchik, J. M. Gohlke, S. Wang, and M. B. Richardson. “Methods for estimating wet bulb globe temperature from remote and low-cost data: A comparative study in central Alabama.” In *GeoHealth*, vol. 4, issue 5. 16 pp. 24 April 2020.

$$B = S\left(\frac{f_{db}}{4\sigma\cos(\theta)} + \left(\frac{1+\alpha_{sfc}}{\sigma}\right) f_{dif}\right) + (\varepsilon_a)T_a^4$$

$$C = \frac{hu^{0.58}}{\varepsilon_g \sigma}$$

T_g = globe temperature (°C)
T_a = air temperature (°C)
S = incoming solar radiation (W m^{-2})
f_{db} = direct beam radiation fraction (from 0 to 1)
σ = Stefan-Boltzmann constant
θ = sun zenith angle (degrees)
α_{sfc} = surface albedo
f_{dif} = diffuse radiation fraction ($1 - f_{db}$; from 0 to 1)
ε_a = thermal emissivity of the air
h = convective heat transfer coefficient (W m^{-2} °C^{-1} [hr m^{-1}]$^{0.58}$)
ε_g = BG emissivity
u = wind speed (m hr^{-1})

Values for ε_a, ε_g, α_g, and f_{db} are the same as those used in Liljegren, α_{sfc} was set to 0.2, and a minimum wind speed of 1 m s^{-1} (3600 m hr^{-1}) was applied. Dimiceli and Piltz used h = 0.315 for all observations. Based on measured T_g collected at five Army test ranges between 2014 and 2018, more accurate T_g estimations using the Dimiceli method were obtained when h is set to 0.228 during the day and 0 at night (with day/night differentiation at 87° zenith angle). These h values are used by the NWS in its NDFD and National Blend of Models calculations as of November 2024. The quality of measured T_g used to derive the 0.228 h_{day} value was uncertain due to varying globe characteristics and sensor positioning that can affect measurements. New h values were calculated from the 2021 T_g data obtained from Campbell Scientific BLACKGLOBE-L sensors with similar configurations. The variation in average and median h values across the participants (Table 2) is quite large, though lower (higher) values were generally found at dry (more humid) locations. The average and median h_{day} values were used as initial guides for finding a constant h_{day} value that gives the best statistical results from the Dimiceli BG model when considering the entire 2021 dataset. Based on minimizing the mean absolute error (MAE) and maximizing the number of estimations with errors of ±2 °C, the best results occurred when h_{day} = 0.207. The BG observations from Hennepin County and Redstone Test Center were excluded for the analysis as the temperature probe in the BG was installed differently than other ranges, leading to biases in the measured T_g.

Table 2. Heat Transfer Coefficient Values

Location	**Average**	**Median**
Aberdeen Test Center	0.242	0.203
China Lake	0.164	0.153
Cold Regions Test Center	0.212	0.170
Dugway Proving Ground	0.204	0.173
Edwards AFB	0.153	0.151

Eglin AFB	0.218	0.181
Hennepin County	0.296	0.249
North Carolina ECONet	0.271	0.216
Pacific Missile Range Facility	0.191	0.168
Redstone Test Center	0.328	0.262
Vandenberg SFB	0.232	0.192
White Sands Test Center	0.148	0.126
Yuma Proving Ground	0.148	0.126
Orange – dry; Green – humid		

While the BG heat energy balance equations used by Liljegren and Dimiceli are slightly different, they do contain the same general energy loss and gain elements. Inspection of individual sections of the equations reveals that the Liljegren form of the heat gain terms can be substituted in for those same terms in Dimiceli. This substitution changes the variable *B* in the Dimiceli BG algorithm to the following.

$$B = S\left(\frac{f_{db}}{4\sigma\cos(\theta)} + \left(\frac{1 - f_{db} + \alpha_{sfc}}{2\sigma}\right)\right) + \frac{1}{2}(1 + \varepsilon_a)T_a^4 \qquad \text{Equation 4}$$

Even though *B* has changed, the general form of the Dimiceli BG estimation equation (Equation 3) remains the same since the linearization process only involved the variable *C*. However, the change in *B* requires calculation of a new heat transfer coefficient value. Using a random dataset containing 70% of daytime observations for all sites (excluding Hennepin County and Redstone), an h_{day} value of 0.167 provided the best statistical results.

The MAE and bias statistics over the course of the day (Figure 3) show considerable differences in the BG models. The original Dimiceli model with h = 0.315 throughout the day (Dim315) gave the worst results with MAE reaching up to 3.5 °C at midday. The MAE also peaked around midday for the Liljegren model (Lil) with maximum values around 2.4 °C. The mean bias for Liljegren was positive throughout the day, reaching a maximum of ~2 °C at midday. The three adjusted Dimiceli models (Dim228 for h_{day} = 0.228 and h_{night} = 0; Dim207 for h_{day} = 0.207 and h_{night} = 0; Dim167L for h_{day} = 0.167 and h_{night} = 0 and using Equation 4 for the *B* term) have smaller MAE than Liljegren in the 09 to 13 LST hours and lesser mean bias throughout the day. The MAE for Dim228 and Dim207 may be higher than Liljegren during the early to mid-morning and again in the late afternoon due in part to differences in representing heat gain terms. The Dim167L model uses the Liljegren form of these terms with the resulting MAE values similar to the Liljegren BG model. Peak MAE values in Dim167L reach around 1.2 °C (~1 °C less than Liljegren) with only a slight mean bias during the day. The Dim167L MAE is higher at night compared to the other Dimiceli models and Liljegren with a notable positive mean bias.

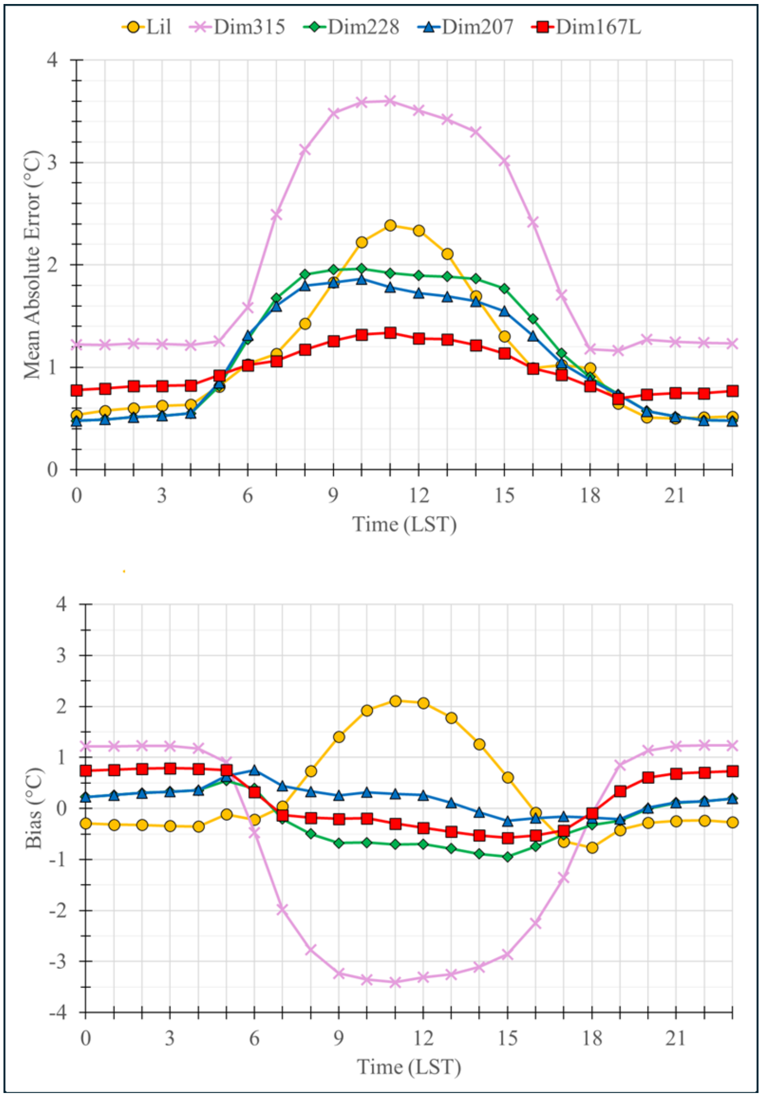

Figure 3. BG Temperature Estimation MAE (top) and Bias (bottom) by Hour

Model errors binned by measured T_g (Figure 4) show Liljegren with a general warm bias and very large spread in errors while the Dimiceli-based estimation methods have a cool bias that increases in magnitude with increasing T_g when T_g >30 °C. Dim167L has the smallest MAE overall in that higher T_g range. At T_g < 30 °C, MAE is nearly the same for all models with Liljegren exhibiting a slight cool bias and the Dimiceli-based models showing a slight warm bias.

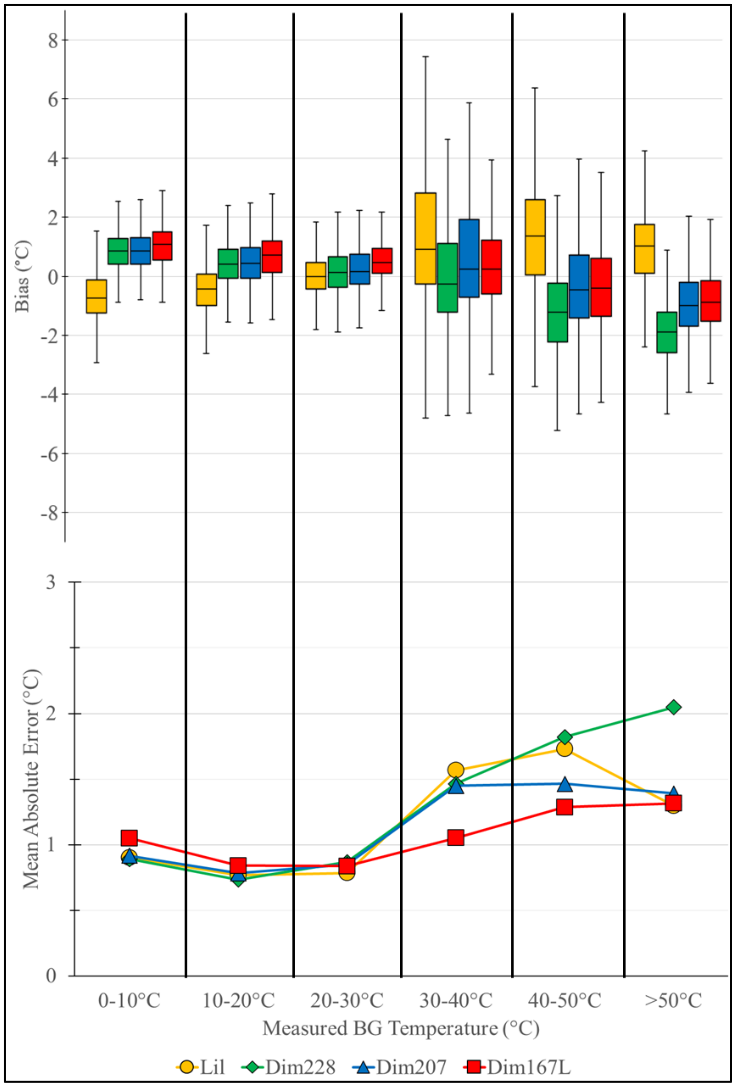

Figure 4. BG Temperature Estimation Bias (Top) and MAE (Bottom) by Measured BG Temperature Bins

The Dim167L model rates best in percentage observations within 2 °C of the measured T_g, especially during daytime hours (Table 3). The warm bias in Liljegren stands out with a higher percentage of observations in the 2-4 °C bin compared to other methods. The distribution of observations is skewed a bit toward the cool side for Dim228 and Dim167L while Dim207 has a very slight skewness towards the warm bias bins.

Table 3. Percentage Distribution of BG Errors

Error	All				Daytime			
	Liljegren	Dim228	Dim207	Dim167L	Liljegren	Dim228	Dim207	Dim167L
< −4 °C	0.1%	2.5%	1.0%	0.8%	0.4%	5.0%	2.1%	1.7%
−4 °C to −2 °C	3.5%	8.7%	5.4%	5.6%	5.5%	17.1%	10.3%	11.2%
−2 °C to 2 °C	83.0%	83.2%	84.9%	89.0%	66.8%	67.1%	70.6%	81.3%
2 °C to 4 °C	12.6%	4.5%	6.4%	4.3%	22.4%	8.4%	12.2%	5.2%
> 4 °C	0.8%	1.1%	2.3%	0.3%	4.9%	2.3%	4.8%	0.5%

Table A-1 contains a comparison of model predictions with measured T_g data by location. Differences between models will vary by location given the different climate characteristics that affect the convective heat transfer coefficient. Most locations have better statistical results with the Dim167L method versus Liljegren, especially those in more humid locations. The Dim207 method also offers an improvement over Liljegren at most locations.

3.2 NWB Temperature

The Liljegren NWB algorithm is a physical model based on the heat energy balance of a wetted wick. The balance equation can be arranged to solve for T_{nwb} (Equation 5):

$$T_{nwb} = T_a - \frac{\Delta H}{c_p}\frac{M_{H2O}}{M_{Air}}\left(\frac{Pr}{Sc}\right)^a\left(\frac{e_w - e_a}{P - e_w}\right) + \frac{\Delta F_{net}}{A\ h} \qquad \text{Equation 5}$$

where

T_{nwb} = natural wet-bulb temperature (K)
T_a = air temperature (K)
ΔH = heat of vaporization
c_p = specific heat at constant pressure
M_{H2O} = molecular weight of water vapor
M_{Air} = molecular weight of air
Pr = Prandtl number
Sc = Schmidt number
a = constant (0.56)
e_w = vapor pressure at the NWB temperature (hPa)
e_a = vapor pressure at the air temperature (hPa)
P = atmospheric pressure (hPa)
ΔF_{net}= net radiative gain by the wick
A = surface area of the wick (m)
h = convective heat transfer coefficient (W m^{-2} K^{-1})

Definitions and values for the variables above can be found in Liljegren et al. and are used in the calculations for this paper. Wind speed is accounted for in the value of h. An iterative process is used to solve for T_{nwb} with the dew point temperature as the first guess.

The Hunter and Minyard NWB model was constructed by linearly regressing incoming solar radiation and wind speed on the difference between T_{nwb} and the psychrometric wet-bulb temperature T_w. The regression equation given in Equation 3 of Hunter and Minyard does not specify units for T_{nwb} and T_w, though Hunter[18] clarifies that the coefficients have units that provide a result in Fahrenheit temperature. Coefficients were derived from a small dataset (15-minute observations during a four- to six-hour period from 0900-1500 LST over nine days

[18] C. H. Hunter. "A Modified Heat Stress Algorithm for Partially Enclosed Structures." WSRC-RP-2001-01097. U.S. Department of Energy, Office of Scientific and Technical Information, Oak Ridge, TN. 2001. Retrieved 22 January 2025. Available at https://sti.srs.gov/fulltext/rp20011097/rp20011097.html.

spanning May-July 1999) at one location (interior South Carolina). The coefficients provided in Equation 6 are converted values to provide a result in Celsius temperature.

$$T_{nwb} = T_w + 0.00117S - 0.233u + 1.072 \quad \text{Equation 6}$$

where

T_{nwb} = NWB temperature (°C)
T_w = psychrometric wet-bulb temperature (°C)
S = incoming solar radiation (W m^{-2})
u = wind speed (m s^{-1})

The BP algorithm uses conditional states of the difference between T_g and air temperature T_a as well as the wind speed u for estimating T_{nwb} (Equation 7a and 7b):

$$\text{If } T_g - T_a \leq 4\text{ °C}: T_{nwb} = T_a - \delta\,(T_a - T_w) \quad \text{Equation 7a}$$

where

$\delta = 0.85$ for $u < 0.03$ m s^{-1}
$\delta = 1.0$ for $u > 3$ m s^{-1}
$\delta = 0.96 + 0.069 \log_{10} u$ for $0.03 \leq u \leq 3$ m s^{-1}

$$\text{If } T_g - T_a > 4\text{ °C}: T_{nwb} = T_w - 0.2 + 0.25\,(T_g - T_a) + \varepsilon \quad \text{Equation 7b}$$

where

$\varepsilon = 1.3$ for $u < 0.1$ m s^{-1}
$\varepsilon = 0.1$ for $u > 1$ m s^{-1}
$\varepsilon = 0.1 / u^{1.1}$ for $0.1 < u < 1$ m s^{-1}

Finding Improvements noted that adding effects of heat transfer between the air and the wick on the temperature sensor to the other elements used in the HM model would improve the estimate of T_{nwb}. The heat transfer effect can be accounted for using the wet-bulb depression (T_{wd}). A new model (Equation 8) was derived using observed data from 15 May to 15 June 2021 collected at six of the RCC-MG data collection campaign locations.

$$T_{nwb} = T_w + 0.001651S - 0.09555u + 0.13235T_{wd} + 0.20249 \quad \text{Equation 8}$$

where

T_{nwb} = NWB temperature (°C)
T_w = psychrometric wet-bulb temperature (°C)
S = incoming solar radiation (W m^{-2})
u = wind speed (m s^{-1})
T_{wd} = wet-bulb depression (°C).

The mean bias of the estimations from Equation 8 exhibited a wave pattern over the daytime period for locations with good T_{nwb} one-minute data presented in Figures 17-19 of *Finding Improvements*. This wave pattern suggests effects of one or more of the variables in the T_{nwb} estimation are nonlinear. Scatterplots of the three variables in Equation 8 versus $T_{nwb} - T_w$ (Figure 5) reveal nonlinear contributions from solar radiation and the wind speed while the contribution from T_{wd} is generally linear.

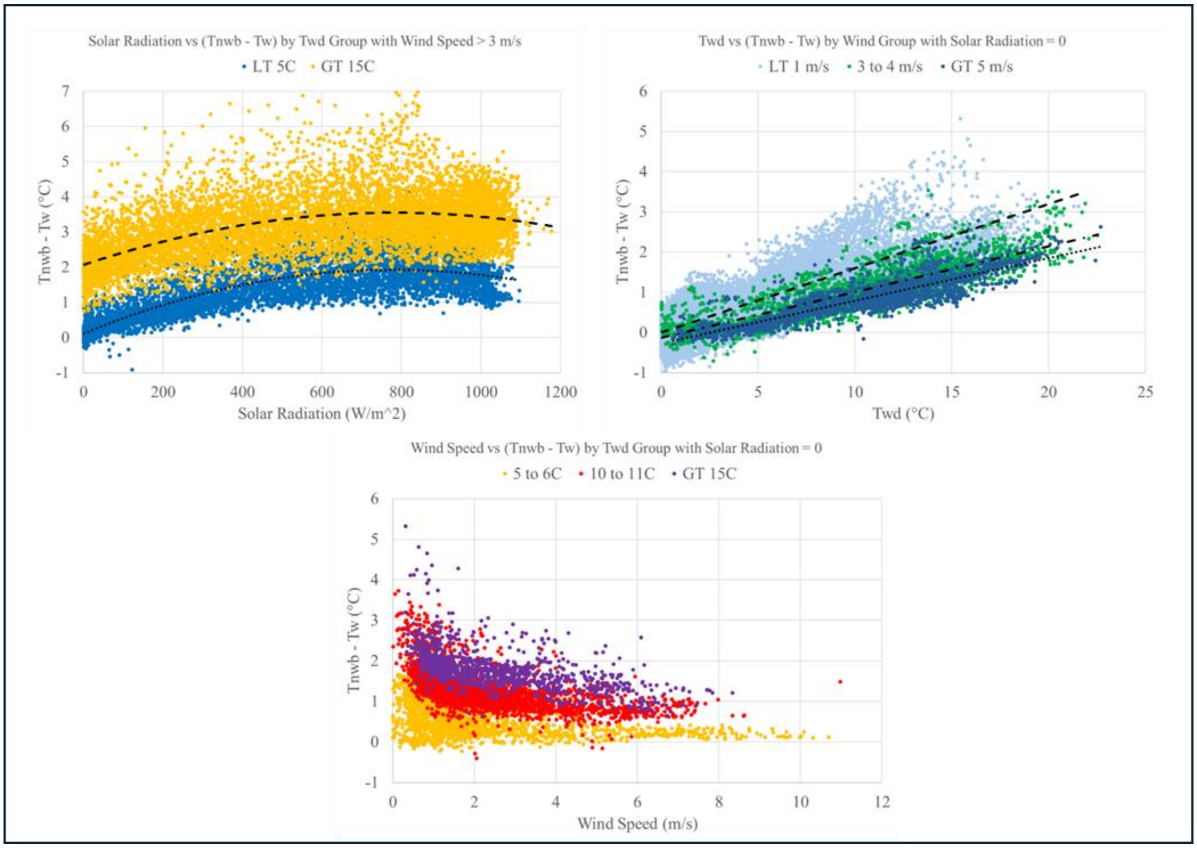

Figure 5. Distribution of Solar Radiation (Top Left), Wet-Bulb Depression (Top Right), and Wind Speed (Bottom) by Difference of the Natural and Psychrometric Wet-Bulb Temperature

The Liljegren NWB equation can be rearranged in the general form $T_{nwb} - T_w = \Delta F_{net} / A\ h$ where ΔF_{net} contains forcings from solar radiation T_{wd} (i.e., heat difference between the air and the wick) that are modulated by the wind speed embedded in the heat transfer coefficient h. The curve best fitting solar radiation versus $T_{nwb} - T_w$ data (for wind speed > 3 m s^{-1}) is a second-order polynomial containing S^2 and S terms with resultant peak $T_{nwb} - T_w$ values around 750 W m^{-2}. The wind speed contribution using data only at night (i.e., $S = 0$) is generally exponential with $T_{nwb} - T_w$ increasing much more quickly with decreasing wind speed below ~1.5 m s^{-1}. A multiple linear regression equation for $T_{nwb} - T_w$ with terms of S^2 / u^x, S / u^x and T_{wd} / u^x was created using a random dataset containing 70% of observations for all locations in the 2021 campaign (excluding Dugway Proving Ground, which had an uncorrectable high bias for unknown reasons) (Equation 9). Different values of the exponent x with the wind speed variable were tested with $x = 0.15$ providing the best statistical results in terms of MAE and error distribution.

$$T_{nwb} = T_w + \left(\frac{-3 \times 10^{-6} S^2 + 0.0046S + 0.135T_{wd}}{u^{0.15}}\right) - 0.0443 \qquad \text{Equation 9}$$

A clear difference in estimation performance is evident in the MAE and mean bias diurnal trends (Figure 6) between the widely used T_{nwb} algorithms from Liljegren (Lil), Hunter and Minyard (HM), and Bernard and Pourmoghani (BP) versus the RCC-derived algorithms currently used by the U.S. NWS and the new algorithm with nonlinear coefficients in Equation 9 (RCCNL). The Lil, HM, and BP models all have quite high MAE, especially during the afternoon when the MAE is near or exceeds 1 °C. The Lil and HM models have a substantial cool bias ranging between −0.5 °C and −1.5 °C throughout much of the day while BP exhibits a slight warm bias up to near 0.7 °C from the mid-morning through mid-afternoon. The MAE in the NWS and RCCNL models is largely between 0.3-0.5 °C, which is generally 0.5-1 °C lower than the other models. The RCCNL model offers slight improvement in MAE over the NWS model given the use of nonlinear coefficients in the estimation. A distinct wave pattern appears in the mean bias for the NWS model while the wave pattern with the RCCNL model is much more subdued.

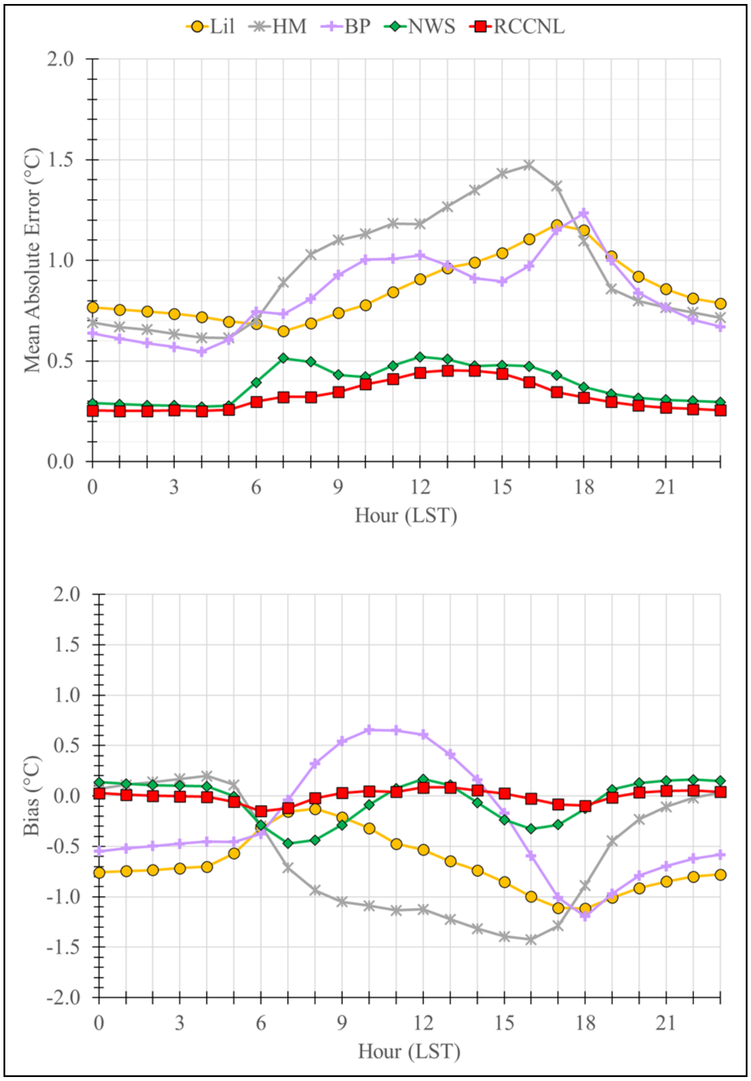

Figure 6. NWB Temperature Estimation MAE (top) and Bias (bottom) by Hour

The substantial cold bias and resultant high MAE in Lil, HM, and BP are driven by poor performance of those models in low RH conditions (Figure 7). The MAE exceeds 1 °C for all three models starting when the RH is below 40% and increases with decreasing RG. Meanwhile, the MAE for the NWS and RCCNL models is ~0.5 °C at these lower RH levels with no clear indication of bias. All models have similar results for RH ≥ 50%, though BP has a 0.2-0.3 °C higher MAE and a much wider range of errors in the 50-80% RH range. HM has a notable high bias above 80%, leading to a slight increase in MAE. NWS and RCCNL have lower MAEs across all RH levels compared to the other models with RCCNL offering slightly better results than NWS.

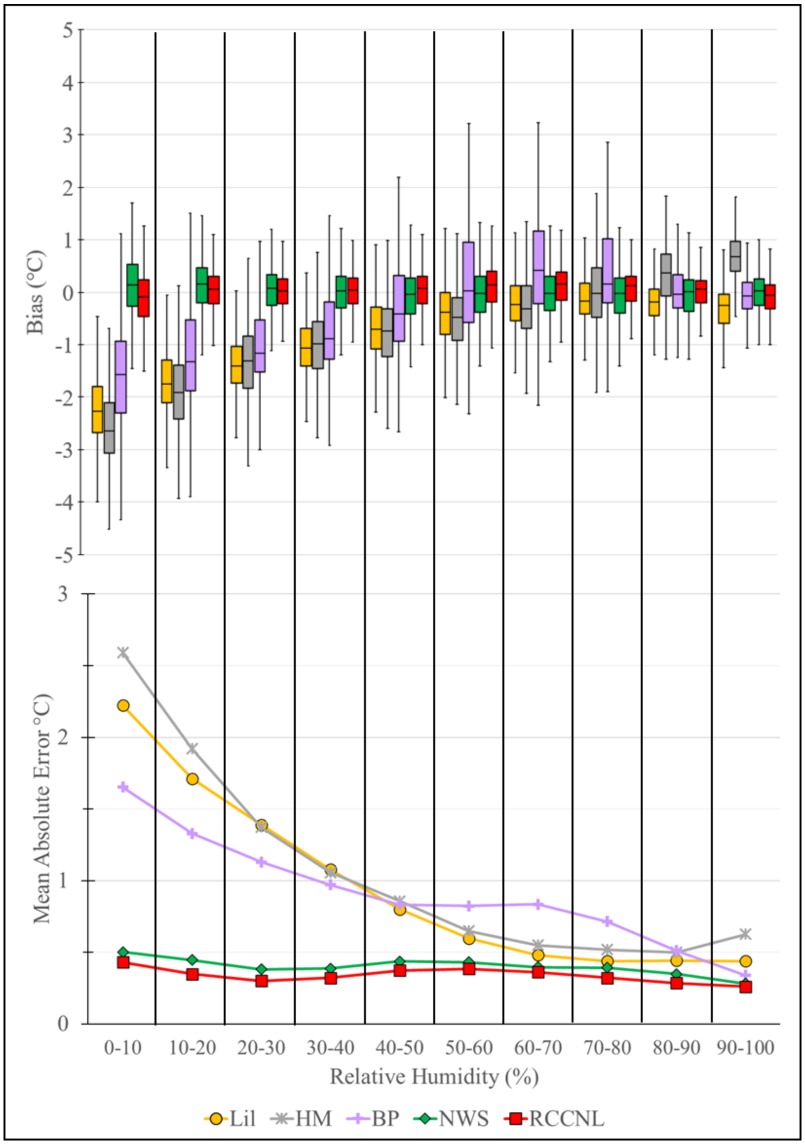

Figure 7. NWB Temperature Estimation Bias (Top) and MAE (Bottom) By RH

Table A-2 has comparisons of model predictions with measured T_{nwb} data by location. Large MAE, negative bias, and larger percentages of observations with greater than 1 °C error mark Lil, HM, and BP for locations with generally lower RH. These models generally perform better at locations with higher RH, though errors are still quite large for HM and BP. The NWS and RCCNL models have much smaller bias (±0.3 °C) and MAE (≤0.5 °C) for all locations with errors exceeding 1 °C in less than 5% of observations for all but three sites (NCECO, RTC, VBG) for NWS and all but one site (VBG) for RCCNL.

3.3 WBGT

Analysis of WBGT estimations included observations with good data from all the standard meteorological variables (air temperature, RH, solar radiation, and wind speed) plus T_g and T_{nwb}. A wide range of temperature and RH conditions were covered by the dataset with a broad normal distribution of temperature centered around 25 °C and a bimodal distribution of RH with peaks at 10-30% and 70-100% (Table 4).

Table 4. Percentage of Observations for WBGT Estimation by Air Temperature and Relative Humidity

		Air Temperature (°C)									
		0-5	5-10	10-15	15-20	20-25	25-30	30-35	35-40	GT 40	Total
Relative Humidity (%)	<10	0.00	0.00	0.00	0.02	0.16	0.48	0.89	1.63	1.01	4.20
	10-20	0.00	0.02	0.11	0.38	1.03	2.15	3.30	2.83	1.44	11.27
	20-30	0.00	0.11	0.44	0.99	2.33	3.21	2.47	1.38	0.84	11.78
	30-40	0.00	0.13	0.57	1.41	2.22	2.39	1.91	0.90	0.02	9.56
	40-50	0.00	0.17	0.60	1.48	1.95	2.16	1.47	0.10	0.00	7.93
	50-60	0.04	0.17	0.78	1.54	1.82	2.24	1.63	0.00	0.00	8.20
	60-70	0.05	0.21	0.91	1.71	2.32	2.69	1.52	0.00	0.00	9.42
	70-80	0.09	0.33	1.12	3.04	2.80	3.27	0.41	0.00	0.00	11.05
	80-90	0.10	0.58	1.82	2.61	3.64	2.80	0.00	0.00	0.00	11.57
	>90	0.22	1.05	6.55	1.68	4.85	0.66	0.00	0.00	0.00	15.02
	Total	0.50	2.78	12.89	14.88	23.13	22.06	13.60	6.85	3.31	

(Blue – Relative Maximum; Red – Relative Minimum)

Estimated WBGT was calculated using the following combination of BG and NWB models (Table 5).

Table 5. WBGT Estimation Methods

WBGT Method	BG	NWB
Liljegren	Equation 2	Equation 5
NWS	Equation 3 with $h_{day} = 0.228$, $h_{night} = 0$	Equation 8
RCCD207	Equation 3 with $h_{day} = 0.207$, $h_{night} = 0$	Equation 9
RCCD167L	Equation 3 with Equation 4 for variable *B;* $h_{day} = 0.167$, $h_{night} = 0$	Equation 9

The NWS, RCCD207, and RCCD167L models have lower MAE than Liljegren with differences largest from the mid-afternoon through the night (Figure 8). Mean bias is near zero for all models from near sunrise until mid-afternoon with Liljegren becoming increasingly biased low in the late afternoon and early evening before leveling off near −0.5 °C during the night. A wave pattern in MAE and bias is present in the NWS model, driven by the errors from NWS NWB. The wave pattern vanishes with the RCCD207 and RCCD167L models that use the RCCNL NWB. The WBGT MAE is lowered by 0.1-0.2 °C when using the Dim167L BG versus the Dim207 BG model with the RCCD167L MAE in the 0.3-0.4 °C range throughout the day.

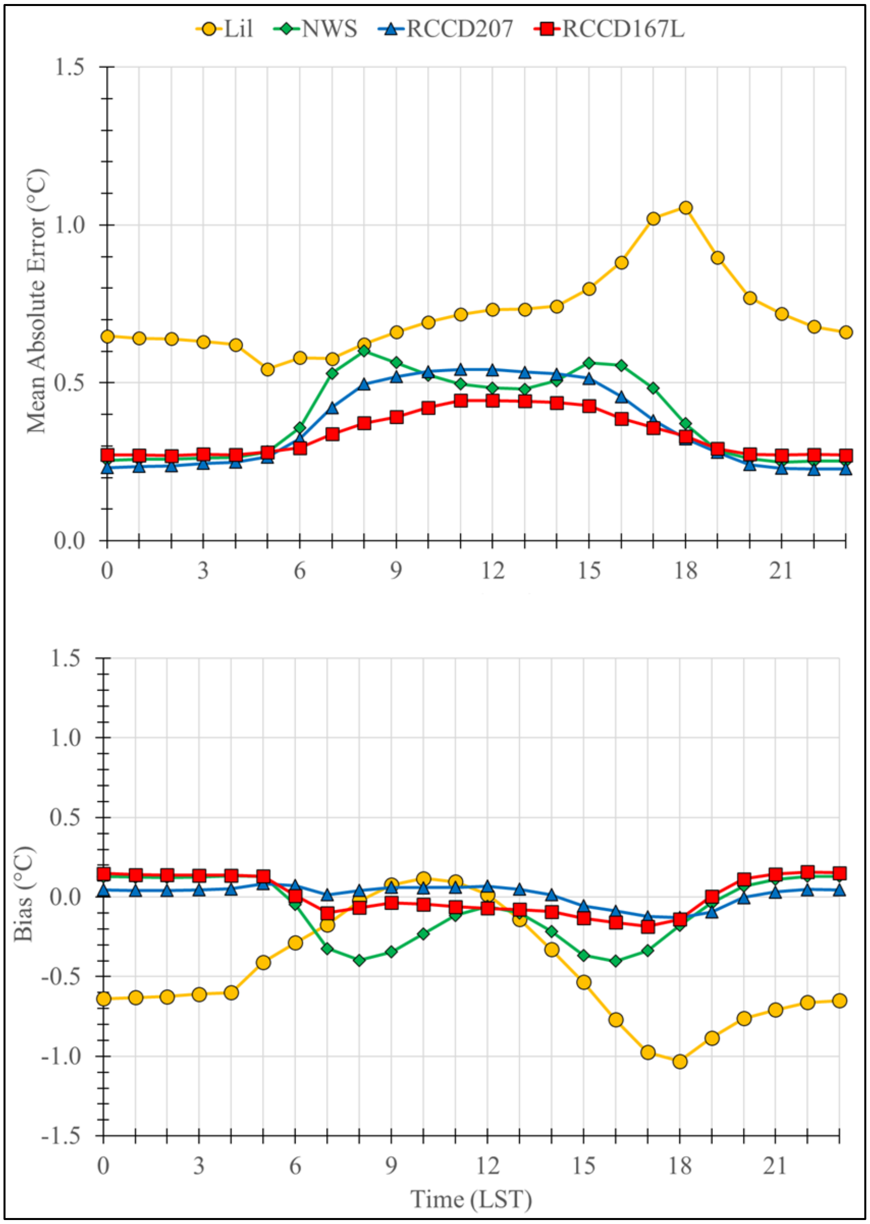

Figure 8. WBGT Estimation MAE (Top) and Bias (Bottom) by Hour

The large negative bias and high MAE in T_{nwb} at low RH from Liljegren carries over to the Liljegren WBGT (Figure 9). The MAE exceeds 1 °C starting in the 20-30% RH range and the upper end of top whisker in the bias chart (1.5 times the interquartile range plus the third quartile value) just reaches zero for RH values below 30%. Liljegren WBGT compares more closely with the other models at higher RH, though the range of errors with Liljegren in those conditions is larger. The MAE and bias for all WBGT estimations with Dimiceli-based BG are very close for all RH conditions, though RCCD167L has a slightly lower MAE and slightly less range in errors for almost all RH conditions.

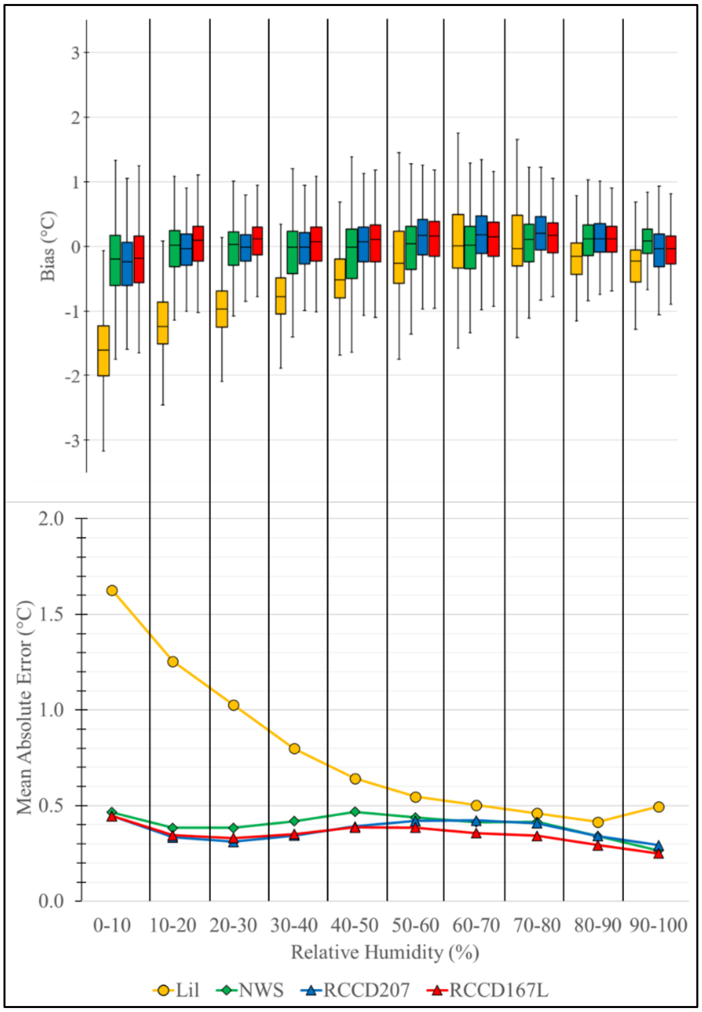

Figure 9. WBGT Estimation Bias (Top) and MAE (Bottom) by RH

When assessing WBGT estimations, it is particularly important to examine algorithm performance when heat conditions reach dangerous levels. Many studies have investigated the frequency and trends of WBGT at certain thresholds, most of which utilize the Liljegren BG and NWB models.[19,20,21 ,22,23] For this paper, heat categories and associated flag colors with respective WBGT ranges are taken from Army Technical Bulletin Medical 507 (Army, "Heat stress…") (Table 6).

[19] Grundstein, A., N. Elguindi, E. Cooper, and M. S. Ferrera. "Exceedance of wet bulb globe temperature safety thresholds in sports under warming climate." In *Clim. Res.*, vol. 58, pp. 183-191, 2013.
[20] Grundstein, A., C. Williams, M. Phan, and E. Cooper. "Regional heat safety thresholds for athletics in the contiguous United States." In *App. Geog.*, vol. 56, pp. 55-60, 2015.
[21] McAllister, C., A. Stephens, and S. M. Milrad. "The heat is on: Observations and trends of heat stress metrics during Florida summers." In *J. App. Meteor. Climatol.*, vol. 61, pp. 277-296. March 2022.
[22] Clark, J., and C. E. Konrad. "Observations and estimates of wet-bulb globe temperature in varied microclimates." In *J. App. Meteor. Climatol.*, vol. 63, pp. 305-319. February 2024.
[23] Davis, B., E. R. Martin, and B. G. Illston. "Climatology of wet-bulb globe temperature and associated heat waves in the U.S. Great Plains." In *J. App. Meteor. Climatol.*, vol. 63, pp. 873-891. August 2024.

Table 6. WBGT Heat Categories	
Heat Category (Flag Condition)	**WBGT Index (°C)**
1 (white)	25.6-27.7
2 (green)	27.8-29.3
3 (yellow)	29.4-31.0
4 (red)	31.1-32.1
5 (black)	> 32.2

Humid and dry locations are grouped separately in evaluating performance of WBGT models at the heat categories (Figure 10) given the difference in NWB model performance based on humidity. For humid locations, Liljegren has a slight high bias for most of the heat categories with the greatest mean bias around 0.5 °C in black flag conditions. The Liljegren MAE increases from 0.5 °C for white flag conditions to 0.7 °C for black flag conditions. The WBGT models with Dimiceli-based BG have biases closer to zero and MAEs from 0.15 °C to 0.4 °C lower than Liljegren. The differences between Liljegren and the other models are more pronounced for dry locations. Liljegren has a −1.0 to −1.5 °C mean bias and corresponding large MAE that is near the range of one heat category on average. Meanwhile, the NWS, RCCD207, and RCCD167L models have biases near zero and MAEs of 0.5 °C or less with RCCD167L slightly outperforming the other models.

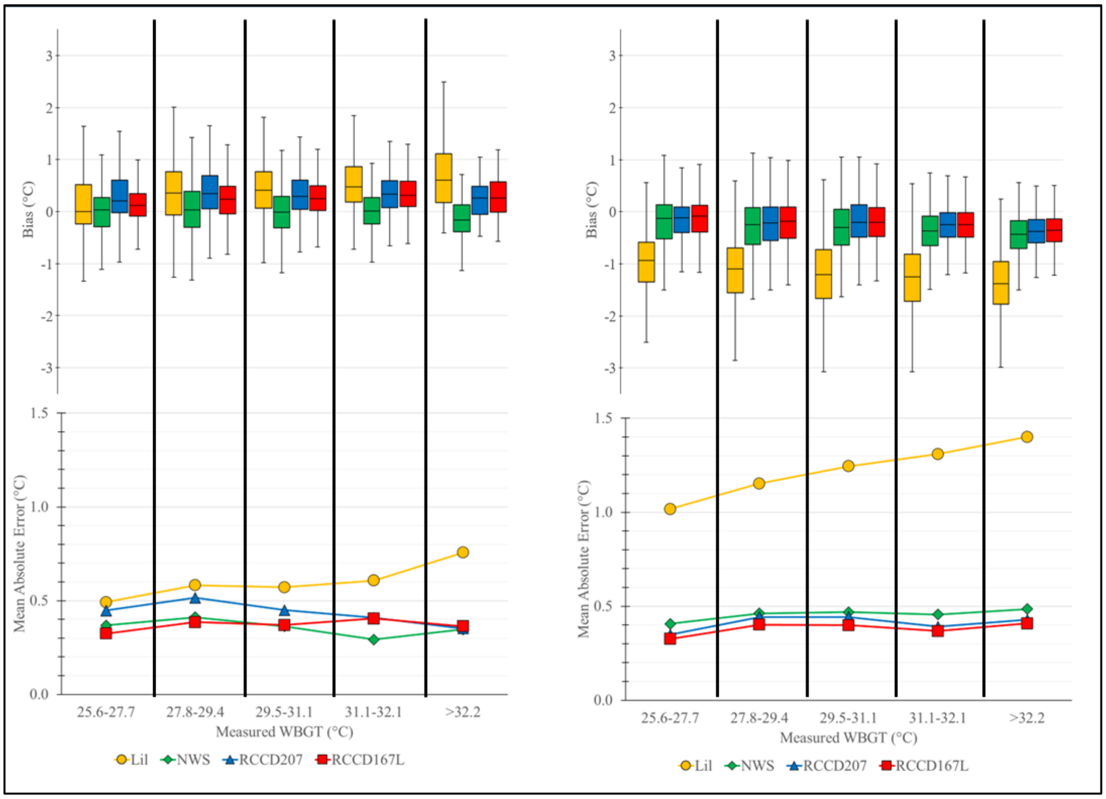

Figure 10. WBGT Estimation Bias (Top) and MAE (Bottom) By Heat Category for Humid (Left) and Dry (Right) Climate Locations

Table A-3 has comparisons of model predictions with measured WBGT data by location. At dry locations, Liljegren has a substantially negative bias and MAE as well as percentage of observations with WBGT >1 °C from measured WBGT exceeding 30%. Differences in WBGT >1 °C are also more frequent with Liljegren than other models at most humid locations. The RCCD167L model provides the best statistical results in terms of lowest MAE and percentage of observations with >1 °C model error.

4. Considerations when Applying WBGT estimations

The psychrometric wet-bulb temperature (T_w) is a crucial component for the accurate estimation of T_{nwb}. Many methods of calculating T_w use an iterative process, including one employed by the NWS in its NDFD (Appendix B) that is used in this paper for the T_w values in T_{nwb} estimations. The comparisons that follow will treat the NWS T_w calculated from the RCC data campaign dataset as truth data. Methods of directly calculating T_w have been developed using various data fit processes. Such methods produce some level of error (when compared to the NWS T_w) that varies by temperature, RH, and pressure. The more sophisticated analytical method from Sadeghi et al.[24] can be applied to locations up to 4500 m mean seal level with reasonably small difference from NWS T_w for most conditions, but average differences greater than 0.5 °C occur when air temperature is greater than 30 °C and/or RH is below 20% (Table 7). Stull[25] developed a regression equation requiring only air temperature and RH to determine T_w, though the expression is technically only valid at standard sea level pressure (1013.25 hPa). Average differences between Stull and NWS T_w become progressively more positive (or less negative) for most conditions as the regression is applied to lower pressures, as evidenced by the differences at Aberdeen Test Center near sea level (Table 8) versus White Sands Test Center at ~1270 m above mean sea level (Table 9). These examples highlight the importance of knowing the limitations and biases of direct T_w calculation methods as non-negligible errors in the estimation of T_{nwb} may be introduced.

Table 7. Average Difference between Sadeghi and NWS T_w (°C)

		Air Temperature (°C)									
		0-5	5-10	10-15	15-20	20-25	25-30	30-35	35-40	40-45	>45
Relative Humidity (%)	<10				0.29	0.38	0.46	0.57	0.65	0.73	0.78
	10-20		0.12	0.17	0.22	0.26	0.30	0.32	0.35	0.37	0.44
	20-30	0.07	0.11	0.14	0.16	0.15	0.13	0.08	−0.05	−0.13	
	30-40	0.06	0.08	0.10	0.10	0.06	−0.01	−0.12	−0.24	−0.33	
	40-50	0.05	0.07	0.07	0.04	−0.02	−0.11	−0.24	−0.33		
	50-60	0.04	0.05	0.04	0.00	−0.07	−0.17	−0.28			
	60-70	0.03	0.03	0.01	−0.03	−0.09	−0.20	−0.28			
	70-80	0.02	0.02	0.00	−0.04	−0.10	−0.18	−0.25			
	80-90	0.01	0.00	−0.01	−0.04	−0.08	−0.13	−0.20			
	>90	0.00	0.00	−0.01	−0.02	−0.04	−0.08				

[24] Sadeghi, S-H., T. R. Peters, D. R. Cobos, H. W. Loescher, and C. S. Campbell. "Direct calculation of thermodynamic wet-bulb temperature as a function of pressure and elevation." In *J. Atmos. Ocean. Tech.*, vol. 30, 1757-1765. August 2013.

[25] Roland Stull. "Wet-bulb temperature from relative humidity and air temperature." In *J. App. Meteor. Climatol.*, vol. 50, pp. 2267-2269. November 2011.

Table 8. Average Difference between Stull and NWS T_w (°C) at ATC

		Air Temperature (°C)							
		<10	10-15	15-20	20-25	25-30	30-35	35-40	>40
Relative Humidity (%)	<10								
	10-20								
	20-30				0.13				
	30-40			−0.11	0.16	0.25	0.43		
	40-50		−0.25	−0.11	0.09	0.26	0.42		
	50-60		−0.31	−0.14	0.02	0.16	0.29		
	60-70		−0.33	−0.20	−0.05	0.08	0.18		
	70-80		−0.30	−0.20	−0.08	0.02	0.10		
	80-90	−0.27	−0.25	−0.15	−0.07	−0.01	0.05		
	>90	−0.17	−0.13	−0.07	−0.02	0.00			

Table 9. Average Difference between Stull and NWS T_w (°C) at WSTC

		Air Temperature (°C)							
		<10	10-15	15-20	20-25	25-30	30-35	35-40	>40
Relative Humidity (%)	<10			0.30	0.24	0.32	0.50	0.75	1.02
	10-20		0.48	0.52	0.59	0.80	1.01	1.18	
	20-30	0.30	0.40	0.58	0.76	0.96	1.19	1.32	
	30-40	0.26	0.30	0.47	0.65	0.87	1.04	1.25	
	40-50		0.20	0.31	0.50	0.67	0.83		
	50-60		−0.01	0.17	0.34	0.47			
	60-70		−0.09	0.04	0.18	0.28			
	70-80		−0.16	−0.04	0.05				
	80-90		−0.15	−0.06	−0.01				
	>90	−0.15	−0.11	−0.04	−0.02				

The algorithms presented in this paper depend on solar radiation data. Most weather observation platforms in the DoD (and in general) do not measure solar radiation. Options are available to approximate solar radiation using other sensors or numerical weather prediction model data. Several studies have used sky condition measured at many airfields plus expected maximum solar radiation for a given time of day.[26,27] Conversion of light intensity (i.e., illuminance) to solar irradiance has provided reasonable estimates.[28] Illuminance measurements as part of visibility sensors are present in some airfield weather systems, though the raw data is typically inaccessible. Low-cost light sensors could be used for custom-built stations. Solar radiation is available as a direct output variable from many numerical weather prediction models or can be estimated using model cloud cover. An application developed by the Army Research

[26] Kasten, F. and G. Czeplak. "Solar and terrestrial radiation dependent on the amount and type of cloud. In *Sol. Energy*, vol. 24, pp. 177-189. 1980.
[27] Clark, J., C. E. Konrad, and A. Grundstein. "The development and accuracy assessment of wet bulb globe temperature forecasts." In *Wea. Forecasting.*, vol. 39, pp. 403-419. February 2024.
[28] Michael, P. R., D. E. Johnson, and W. Moreno. "A conversion guide: solar irradiance and lux illuminance." In *J. Measure. Eng.*, vol. 8, issue 4, pp. 153-166. December 2020.

Laboratory[29] produces an estimated solar radiation value based on cloud coverage, cloud type, location, and time of day. Use of sun angle as a replacement for solar radiation has also been examined.[30]

The Dimiceli and Liljegren BG models require calculation of direct beam fraction (f_{db}). For this paper, direct beam fraction was determined using Equations 13 and 14 of Liljegren et al. Those equations require actual solar radiation (or reasonable estimates of actual solar radiation) and the maximum expected solar radiation based on latitude and earth-sun distance. The NWS also uses maximum expected solar radiation, but it determines f_{db} by multiplying cloud cover (0 to 1) by the expected solar radiation value (Boyer). Calculations can be simplified if a constant f_{db} is implemented, such as in Hunter and Minyard. The MAE for the Dim167L BG model with f_{db} = 0.67, f_{db} = 0.75 and f_{db} from Liljegren are very close from mid-morning through late afternoon (Figure 11). The MAE is considerably larger for algorithms using constant f_{db} in the first couple hours after sunrise with a period of slightly larger errors just before sunset. These errors arise as periods near sunrise and sunset tend to have actual f_{db} value that are quite small. The larger errors using a constant f_{db} value may be acceptable early in the day given the lesser levels of heat stress during that period.

[29] David Sauter. "A wet-bulb globe temperature validation study using standard meteorological inputs and modeled solar irradiance." *J. Operational Meteor*., vol. 1, pp. 215-225. 13 November 2013.
[30] Biggar, D. G., P. B. Homan, T. A. Russ, K. D. Burris, and M. D. Scott. "Development of a Wet Bulb Globe Temperature approximation equation from standard meteorological variables and implementation of an automated heat stress condition display at the Eglin Range." Paper presented during the Ninth Conference on Environment and Health, Austin, TX., 8-10 January 2018.

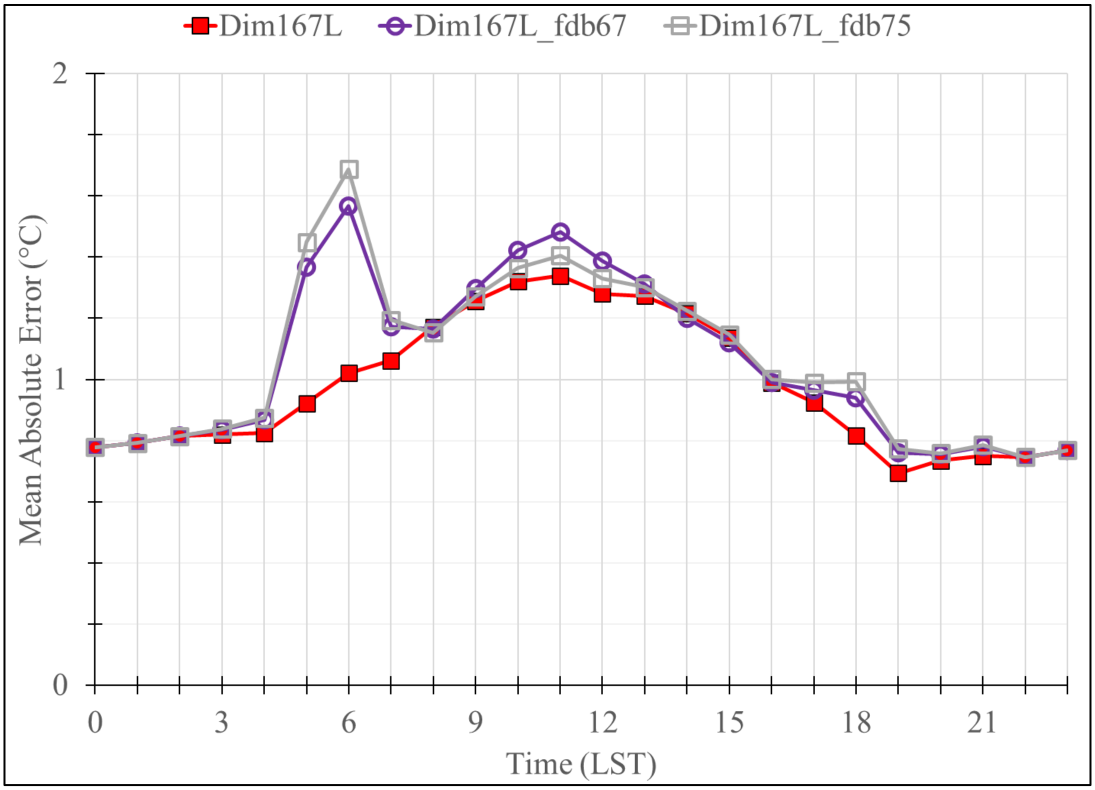

Figure 11. MAE by Hour of Modified Dimiceli BG Estimation Using Different Values of Direct Beam Radiation Fraction

5. Summary

The RCC-MG conducted a campaign in 2021 to collect a high-quality observational WBGT dataset to verify the most widely used T_g and T_{nwb} estimation algorithms and to develop improved algorithms with simpler calculations with reasonably accurate solutions using standard meteorological data. New T_g and T_{nwb} estimation algorithms developed from the campaign dataset provide simpler calculations and improved WBGT estimations with errors generally less than from Liljegren. These new algorithms can be applied at any location with observed or modeled temperature, humidity, wind, solar radiation, and pressure data. Estimates of T_g from Liljegren tended to have a high bias (up to 2 °C at midday) while the Dimiceli BG model with h_{day} = 0.228 and h_{night} = 0 used by the NWS is biased low (generally between 0.5 °C and 1.0 °C). An adjustment to h_{day} = 0.207 in Dimiceli improved the estimations with additional further improvement when using the Liljegren representation of heat gain expressions in the variable *B* in Dimiceli using h_{day} = 0.167. Liljegren and HM T_{nwb} estimations performed well with RH > 50% but each develop a substantial low bias starting around 40% RH that increases with decreasing RH. The BP NWB has a slight high bias at RH > 50%, though the range in errors is quite large between 50% and 80% RH. Like Liljegren and HM, BP has a substantial low bias when RH < 40% that increases with decreasing RH. The T_{nwb} estimate developed from the first month's data from the 2021 RCC-MG campaign and in use by the NWS operationally has little bias across all RH values and the MAE is lower than that for the Liljegren, HM, and BP algorithms. A new regression with nonlinear coefficient values using a larger portion of the 2021 RCC-MG dataset gives slightly improved results from the earlier RCC-MG algorithm and has a mean bias near zero throughout the day. Although Liljegren produces WBGT values with a relatively small amount of error, the seemingly good data are a result of high T_g values being offset by low T_{nwb} values.

APPENDIX A

Tables of WBGT Estimation Algorithm Statistics by Location

Table A-1. BG Temperature

Location	Count	Liljegren			Dim228			Dim207			Dim167L		
		Bias	MAE	ΔBG>2 °C	Bias	MAE	ΔBG>2 °C	Bias	MAE	ΔBG>2 °C	Bias	MAE	ΔBG>2 °C
ATC	12,353	0.60	1.33	25.4%	0.31	0.93	12.1%	0.77	1.10	16.3%	0.43	0.81	8.0%
CL	8051	−0.63	0.92	6.5%	−0.24	0.71	4.6%	−0.13	0.68	4.3%	0.56	0.81	2.5%
CRTC	9998	−0.78	1.06	15.0%	−0.67	1.70	32.6%	−0.32	1.61	32.8%	−0.69	1.44	28.4%
DPG	10,089	0.02	1.22	18.2%	−0.03	1.04	13.3%	0.39	0.98	11.5%	0.50	0.95	7.2%
EDW	12,210	0.48	0.83	13.6%	−0.54	0.94	11.2%	−0.16	0.73	5.7%	0.18	0.71	4.2%
EGL	7494	0.68	0.90	17.3%	0.12	0.84	9.2%	0.43	0.81	9.8%	0.18	0.65	2.6%
HEN	---	---	---	---	---	---	---	---	---	---	---	---	---
NCECO	13,096	1.03	1.56	29.0%	0.69	1.06	15.2%	1.15	1.31	21.5%	0.86	1.02	13.1%
PMRF	2175	0.64	1.02	19.1%	−0.23	1.10	17.9%	0.14	0.99	13.9%	−0.07	1.00	8.8%
RTC	---	---	---	---	---	---	---	---	---	---	---	---	---
VBG	14,043	0.29	1.39	20.9%	−0.12	1.01	13.0%	0.23	0.92	10.3%	0.08	0.61	3.3%
WSTC	13,715	0.02	0.90	11.5%	−0.92	1.74	34.8%	−0.55	1.49	29.2%	−0.39	1.60	29.4%
YPG	14,473	0.36	0.80	9.6%	−0.48	1.14	16.4%	−0.10	0.91	8.2%	0.17	0.98	8.3%

Table A-2. NWB Temperature

Location	Count	Liljegren			Hunter & Minyard			Bernard & Pourmoghani			RCC-NWS			RCC Nonlinear (RCCNL)		
		Bias	MAE	ΔNWB>1 °C	Bias	MAE	ΔNWB>1 °C	Bias	MAE	ΔNWB>1 °C	Bias	MAE	ΔNWB>1 °C	Bias	MAE	ΔNWB>1 °C
ATC	12,353	0.01	0.40	6.9%	0.23	0.52	11.3%	0.47	0.70	27.4%	0.10	0.27	0.9%	0.18	0.26	0.3%
CL	8051	−1.76	1.48	94.4%	−1.17	1.40	49.7%	−1.49	1.21	80.5%	0.12	0.41	2.5%	0.02	0.33	2.4%
CRTC	9998	−0.15	0.43	8.0%	−0.32	0.94	45.2%	0.02	0.42	6.8%	−0.07	0.41	3.5%	0.13	0.30	0.2%
DPG	---	---	---	---	---	---	---	---	---	---	---	---	---	---	---	---
EDW	12,210	−1.20	1.23	61.5%	−1.43	1.48	63.1%	−0.87	0.98	46.7%	0.16	0.38	3.6%	0.12	0.29	1.3%
EGL	7494	−0.21	0.25	1.2%	0.13	0.54	3.9%	0.21	0.43	15.3%	0.04	0.21	0.2%	0.12	0.18	0.1%
HEN	9192	0.03	0.51	9.9%	0.17	0.54	11.9%	0.42	0.65	25.8%	0.13	0.36	3.3%	0.24	0.36	3.9%
NCECO	13,096	−0.46	0.70	21.8%	−0.19	0.51	13.2%	0.05	0.81	26.3%	−0.29	0.48	7.8%	−0.22	0.44	4.2%
PMRF	2175	−0.18	0.21	0.0%	0.11	0.44	<0.1%	0.36	0.56	22.9%	0.28	0.34	2.7%	0.31	0.32	<0.1%
RTC	8758	−0.12	0.38	9.1%	0.21	0.85	43.1%	0.41	0.56	20.4%	−0.08	0.38	6.4%	−0.02	0.29	3.8%
VBG	14,043	−0.41	0.61	11.7%	−0.12	0.69	21.0%	0.06	0.63	20.7%	−0.36	0.50	11.4%	−0.32	0.42	6.4%
WSTC	13,715	−1.09	1.13	53.0%	−1.03	1.16	51.5%	−0.71	0.95	40.8%	0.08	0.38	4.7%	0.03	0.31	2.3%
YPG	14,473	−1.67	1.67	80.5%	−1.53	1.54	65.5%	−1.29	1.35	63.1%	−0.09	0.35	4.5%	−0.15	0.30	3.1%

Table A-3. WBGT

Location	Count	Liljegren			Dim228 & RCC-NWS			Dim207 & RCCNL			Dim167L & RCCNL		
		Bias	MAE	ΔWBGT>1 °C	Bias	MAE	ΔWBGT>1 °C	Bias	MAE	ΔWBGT>1 °C	Bias	MAE	ΔWBGT>1 °C
ATC	12,353	0.13	0.51	13.9%	0.13	0.31	2.2%	0.22	0.36	3.7%	0.21	0.30	1.3%
CL	8051	−1.35	1.36	84.7%	0.04	0.22	0.9%	0.06	0.23	1.2%	0.13	0.24	1.3%
CRTC	9998	−0.26	0.44	8.4%	−0.18	0.59	19.6%	−0.11	0.50	16.0%	−0.04	0.45	6.6%
DPG	---	---	---	---	---	---	---	---	---	---	---	---	---
EDW	12,210	−0.74	0.80	29.4%	0.00	0.32	3.0%	0.08	0.26	1.6%	0.12	0.29	0.4%
EGL	7494	−0.01	0.22	1.1%	0.05	0.25	0.7%	0.11	0.24	1.1%	0.12	0.20	0.3%
HEN	---	---	---	---	---	---	---	---	---	---	---	---	---
NCECO	13,096	−0.11	0.68	14.3%	−0.06	0.37	5.6%	0.03	0.43	7.0%	0.02	0.36	3.9%
PMRF	2175	0.00	0.25	0.9%	0.15	0.34	1.5%	0.23	0.32	1.2%	0.21	0.29	0.0%
RTC	---	---	---	---	---	---	---	---	---	---	---	---	---
VBG	14,043	−0.23	0.60	10.1%	−0.27	0.45	9.8%	−0.20	0.40	7.7%	−0.21	0.36	4.0%
WSTC	13,715	−0.76	0.81	33.1%	−0.13	0.50	12.6%	−0.05	0.43	9.6%	−0.06	0.44	7.3%
YPG	14,473	−1.09	1.10	51.2%	−0.16	0.37	4.3%	−0.08	0.31	2.5%	−0.07	0.31	1.7%

APPENDIX B

Calculation of NWS Psychrometric Wet-Bulb Temperature

Below is Python code for the calculation of the psychrometric wet-bulb temperature (T_w) used by the U.S. NWS in its NDFD. Functions for saturated vapor pressure and dew point temperature that are part of the T_w calculation are included at the end of this section.

```
def TwNatlWS(Tair, rh, pres):

    phase = 0
    TairK = Tair + 273.15
    vpair = (rh / 100) * esat(TairK, phase)             #Actual vapor pressure to get to dew point
    Tdew = dew_point(vpair, phase) - 273.15   #Dew point in degrees Celsius (liquid water phase)

    #Constants
    c1 = 0.0091
    c2 = 6106.4

    fp = 0.0006355 * pres
    es = 6.11 * 10**((Tair * 7.5) / (Tair + 237.3))
    ed = 6.11 * 10**((Tdew * 7.5) / (Tdew + 237.3))
    s1 = es - ed
    s2 = Tair - Tdew

    if s2 == 0: Twc = Tair
    else: Twc = ((Tair * fp) + (Tdew * (s1 / s2))) / (fp + (s1 / s2))

    iterations = 0
    while iterations < 5:
        Twk = Twc + 273.15
        ew = 6.11 * 10**(((Twc * 7.5) / (Twc + 237.3)))
        de1 = fp * (Tair - Twc)
        de = de1 - (ew - ed)
        der = ((ew * (c1 - (c2 / (Twk**2))) - fp))
        Twk = Twk - (de / der)
        Twc = Twk - 273.15
        iterations += 1

    return Twc, Tdew
-------------------------------

def esat(Tk, phase):

   ' tk = air temperature, K
```

```
    if phase == 0:
        Y = (Tk - 273.15) / (Tk - 32.18)
        es = 6.1121 * np.exp(17.502 * Y)
    else:
        Y = (Tk - 273.15) / (Tk - 0.6)
        es = 6.1115 * np.exp(22.452 * Y)

    es = 1.004 * es
    return es
-------------------------------

def dew_point(e, phase):

    ' e = vapor pressure, mb

    if phase == 0:          #dew point
      z = np.log(e / (6.1121 * 1.004))
      tdk = 273.15 + (240.97 * z) / (17.502 - z)
    else:                   #frost point
      z = np.log(e / (6.1115 * 1.004))
      tdk = 273.15 + (272.55 * z) / (22.452 - z)

    dew_point = tdk

    return dew_point
```

APPENDIX C

Citations

Bernard, T. E., and M. Pourmoghani. "Prediction of workplace wet bulb global temperature." In *Appl. Occup. Environ. Hyg.*, vol. 14 issue 2, pp. 126–134.

Biggar, D. G., P. B. Homan, T. A. Russ, K. D. Burris, and M. D. Scott. "Development of a Wet Bulb Globe Temperature approximation equation from standard meteorological variables and implementation of an automated heat stress condition display at the Eglin Range." Paper presented during the Ninth Conference on Environment and Health, Austin, TX., 8-10 January 2018.

Timothy R. Boyer. "NDFD wet bulb globe temperature algorithm and software design." NWS Meteorological Development Laboratory. 8 pp. Retrieved 22 January 2025. Available at https://vlab.noaa.gov/documents/6609493/7858379/NDFD+WBGT+Description+Document.pdf.

Bureau of Labor Statistics, U.S. Department of Labor. It's summer and it's hot on the job. https://www.bls.gov/opub/ted/2024/its-summer-and-its-hot-on-the-job.htm. 20 June 2024. Retrieved 22 January 2025.

Carter, A. W., B. F. Zaitchik, J. M. Gohlke, S. Wang, and M. B. Richardson. "Methods for estimating wet bulb globe temperature from remote and low-cost data: A comparative study in central Alabama." In *GeoHealth*, vol. 4, issue 5. 16 pp. 24 April 2020.

Clark, J., and C. E. Konrad. "Observations and estimates of wet-bulb globe temperature in varied microclimates." In *J. App. Meteor. Climatol.*, vol. 63, pp. 305-319. February 2024.

Clark, J., C. E. Konrad, and A. Grundstein. "The development and accuracy assessment of wet bulb globe temperature forecasts." In *Wea. Forecasting.*, vol. 39, pp. 403-419. February 2024.

Davis, B., E. R. Martin, and B. G. Illston. "Climatology of wet-bulb globe temperature and associated heat waves in the U.S. Great Plains." In *J. App. Meteor. Climatol.*, vol. 63, pp. 873-891. August 2024.

Department of the Air Force. "Thermal Stress Program." DAFI 48-151. 2 May 2022. May be superseded by update. Retrieved 22 January 2025. Available at https://static.e-publishing.af.mil/production/1/af_sg/publication/dafi48-151/dafi48-151.pdf.

Department of the Army. "Heat stress control and heat casualty management." TB MED 507. May be superseded by update. Retrieved 22 January 2025. Available at https://armypubs.army.mil/epubs/DR_pubs/DR_a/ARN35159-TB_MED_507-000-WEB-1.pdf.

Department of the Navy. "Prevention of Heat and Cold Stress Injuries (Ashore, Afloat, and Ground Forces)." Chapter 3 in *Manual of Naval Preventive Medicine*. NAVMED P-5010-3. 12 February 2009. Retrieved 22 January 2025. Available at https://www.med.navy.mil/Portals/62/Documents/BUMED/Directives/All%20Pubs/5010-3.pdf.

Dimiceli, V. E. and S. F. Piltz. "Estimation of black globe temperature for calculation of the WBGT Index." National Weather Service internal technical paper. Retrieved 22 January 2025. Available at https://www.weather.gov/media/tsa/pdf/WBGTpaper2.pdf.

Grundstein, A., N. Elguindi, E. Cooper, and M. S. Ferrera. "Exceedance of wet bulb globe temperature safety thresholds in sports under warming climate." In *Clim. Res.*, vol. 58, pp. 183-191, 2013.

Grundstein, A., C. Williams, M. Phan, and E. Cooper. "Regional heat safety thresholds for athletics in the contiguous United States." In *App. Geog.*, vol. 56, pp. 55-60, 2015.

C. H. Hunter. "A Modified Heat Stress Algorithm for Partially Enclosed Structures." WSRC-RP-2001-01097. U.S. Department of Energy, Office of Scientific and Technical Information, Oak Ridge, TN. 2001. Retrieved 22 January 2025. Available at https://sti.srs.gov/fulltext/rp20011097/rp20011097.html.

Hunter, C. and C. Minyard. "Estimating Wet Bulb Globe Temperature Using Standard Meteorological Measurements." WSRC-MS-99-00757. U.S. Department of Energy, Office of Scientific and Technical Information, Oak Ridge, TN. 1999. Retrieved 22 January 2025. Available at https://digital.library.unt.edu/ark:/67531/metadc620263/m1/

Kasten, F. and G. Czeplak. "Solar and terrestrial radiation dependent on the amount and type of cloud. In *Sol. Energy*, vol. 24, pp. 177-189. 1980.

Lemke., B. and T. Kjellstrom. "Calculating workplace WBGT from meteorological data: A tool for climate change assessment." In *Ind. Health*, vol. 50, pp. 267-278. 2012.

Liljegren, J. C., R. A. Carhart, P. Lawday, S. Tschopp, and R. Sharp. "Modeling the Wet Bulb Globe Temperature Using Standard Meteorological Measurements." In *J. Occup. Environ. Hyg.*, vol. 5, pp. 645-655. 4 August 2008.

Maule, A. L., K. D. Scatliffe-Carrion, K. S. Kotas, J. D. Smith, and J. F. Ambrose. "Heat exhaustion and heat stroke among active component members of the U.S. Armed Forces, 2019-2023." In *Medical Surveillance Monthly Report*, vol. 31, no. 4, pp. 3-8. April 2024.

McAllister, C., A. Stephens, and S. M. Milrad. "The heat is on: Observations and trends of heat stress metrics during Florida summers." In *J. App. Meteor. Climatol.*, vol. 61, pp. 277-296. March 2022.

Michael, P. R., D. E. Johnson, and W. Moreno. "A conversion guide: solar irradiance and lux illuminance." In *J. Measure. Eng.*, vol. 8, issue 4, pp. 153-166. December 2020.

Occupational Safety and Health Administration. “Heat Stress.” Section III, Chapter 4 in OSHA Technical Manual. Retrieved 22 January 2025. Available at https://www.osha.gov/otm/section-3-health-hazards/chapter-4.

Patel, T., S. P. Mullen, and W. R. Santee. “Comparison of methods for estimating wet-bulb globe temperature index from standard meteorological measurements.” In *Military Med.*, vol. 178, pp. 926-933. August 2013.

Range Commanders Council. *Finding improvements in the measurement and estimation of wet-bulb globe temperature*. RCC WP-23-001. August 2023. Retrieved 16 January 2025. Available at https://www.trmc.osd.mil/wiki/x/XQBSDg.

Sadeghi, S-H., T. R. Peters, D. R. Cobos, H. W. Loescher, and C. S. Campbell. “Direct calculation of thermodynamic wet-bulb temperature as a function of pressure and elevation.” In *J. Atmos. Ocean. Tech.*, vol. 30, 1757-1765. August 2013.

David Sauter. “A wet-bulb globe temperature validation study using standard meteorological inputs and modeled solar irradiance.” *J. Operational Meteor*., vol. 1, pp. 215-225. 13 November 2013.

Roland Stull. “Wet-bulb temperature from relative humidity and air temperature.” In *J. App. Meteor. Climatol.*, vol. 50, pp. 2267-2269. November 2011.

Wodzicki, K. R. et al. “Heat stress metrics, trends, and extremes in the southeastern United States.” In *J. App. Meteor. Climatol.*, vol. 63, issue 10, pp. 1137-1156. 01 October 2024.

Yaglou, C. P. and D. Minard. *Prevention of heat casualties at Marine Corps Training Centers*. Office of Naval Research Physiology Branch report, 48 pp. 31 May 1956. Retrieved 22 January 2025. Available at https://apps.dtic.mil/sti/tr/pdf/AD0099920.pdf.

*** * * END OF DOCUMENT * * ***